The International Journal of Advanced Manufacturing Technology (2019) 101:2723–2737
https://doi.org/10.1007/s00170-018-3130-3

ORIGINAL ARTICLE

Microstructure characterization and maximization of the material removal rate in nano-powder mixed EDM of Al-Mg_2Si metal matrix composite—ANFIS and RSM approaches

Mehdi Hourmand[1,2] · Ahmed A. D. Sarhan[3] · Saeed Farahany[4] · Mohd Sayuti[1,2]

Received: 4 August 2018 / Accepted: 21 November 2018 / Published online: 8 December 2018

Abstract
Al-Mg_2Si in situ composite is a new metal matrix composite (MMC) with numerous applications in different engineering fields. MMCs are considered difficult-to-cut materials due to the abrasive nature of the reinforcement (e.g., Mg_2Si), hardness, and built-up edge. Hence, electrical discharge machining (EDM) is one of the alternative ways to machine Al-Mg_2Si. With EDM, it is possible to machine conductive materials with different strength, temperature resistance, and hardness as well as produce complicated shapes, high-aspect ratio slots, and deep cavities with precise dimensions and good surface finish. The experiments in this study were designed by response surface methodology (RSM) and ANFIS was utilized to analyze the nano-powder mixed EDM (NPMEDM) of Al-Mg_2Si in situ composite. The study represents the impacts of NPMEDM parameters on changes in microstructure and material removal rate (MRR). The results revealed that among all interactions, the current-voltage and current-pulse ON time interactions have the most significant effect on MRR. Moreover, current has most significant effect, followed by voltage, pulse ON time and duty factor. An analysis of the Al-Mg_2Si microstructure demonstrated that current, pulse ON time, and voltage have remarkable impact on the microstructure, size of craters, and profile of the machined surface. Moreover, decrease in spark energy leads to less microstructural change and better surface finish.

Keywords Al-Mg_2Si metal matrix composite (MMC) · Nano-powder mixed electrical discharge machining (Nano-powder mixed EDM) · Adaptive neuro-fuzzy inference system (ANFIS) · Response surface methodology (RSM) · Material removal rate (MRR) · Microstructure

1 Introduction

Metal matrix composites (MMCs) are applied widely in diverse fields of engineering. They consist of a soft metal matrix with hard reinforcement materials. The advantages of MMCs over metals include higher specific strength, stiffness, better fatigue resistance, superior wear resistance and lower coefficient of thermal expansion. Al-Mg_2Si in situ composite is an aluminum metal matrix composite (Al-MMC) that has been receiving increasing attention nowadays owing to its enhanced properties that are useful for high-performance applications. Al-20%Mg_2Si in situ composite comprises three important elements, namely aluminum (Al), magnesium (Mg), and silicon (Si) in suitable ratios to attain good properties. Since the Mg_2Si phase reinforcement forms itself during molten metal solidification, the fabricated composite is called "in situ." The shape and size of Mg_2Si reinforcement particles

✉ Mehdi Hourmand
m.hourmand@gmail.com

✉ Ahmed A. D. Sarhan
ahsarhan@kfupm.edu.sa

[1] Center of Advanced Manufacturing and Materials Processing (AMMP), Department of Mechanical Engineering, University of Malaya (UM), 50603 Kuala Lumpur, Malaysia

[2] Department of Mechanical Engineering, University of Malaya (UM), 50603 Kuala Lumpur, Malaysia

[3] Department of Mechanical Engineering, King Fahd University of Petroleum and Minerals, Dhahran 31261, Saudi Arabia

[4] Department of chemical and Materials Engineering, Buein Zahra Technical University, Gazvin 3451745346, Iran

have an important role and influence on the resultant mechanical properties [1, 2].

MMCs are considered difficult-to-cut materials due to the abrasive nature of the reinforcement (e.g., Al-Mg_2Si), hardness and built-up edge [3, 4]. However, electrical discharge machining (EDM) is one of the alternative ways to machine Al-Mg_2Si because there is no contact between the workpiece and electrode [5] and it facilitates the fabrication of high-aspect ratio slots, and deep and complex 3D cavities [5, 6]. EDM is a high-precision modern machining process [7] that removes material from the workpiece as sparks occur between the electrode and workpiece inside the dielectric [8, 9]. The EDM method has been employed extensively for machining conductive materials with different strength, hardness, and temperature resistance [5, 10]. It also has the capability to produce complicated shapes with high accuracy and good surface roughness [5]. Mohal and Kumar [11] found that mixing multi-walled carbon nanotubes with dielectric during EDM of Al-10%SiC_p could improve the MRR by 38.22% and surface finish by 46.06% compared to pure dielectric. Singh et al. [12] reported that adding tungsten powder to dielectric can reduce the tool wear rate (TWR) by up to 51.12% with EDM of AA6061/10%SiC_p composite. In addition, using dielectric with aluminum powder in the EDM process can help enhance the surface roughness and material removal rate (MRR) [13, 14]. However, despite previous findings, Hourmand et al. [15] suggested that using nano-powder with elemental compositions more similar to the workpiece elemental compositions in the dielectric is the best choice due to the migration of nano-powder material to the workpiece.

Copper (Cu) which has precision-drawn sizes is widely available in the market and this material has good electrical conductivity. In order to produce the smoothest surface using EDM, a metallic electrode material should be adopted, like copper, which has the surface finish at least equal to the desired surface finish of workpiece [16]. Electrode with higher melting temperature has better wear resistance in EDM method. For instance, the wear rate of copper is lower than brass because of the higher melting temperature of copper [17]. In the EDM process, the electrode material should be selected based on the workpiece material in order to achieve better performance during machining. In previous research works, copper was selected as an electrode for EDM of Al–MMC with 10% SiC_p [18], 15-35 vol% SiC_p/Al composites [19], Al/Al_2O_3 MMC [20], and Al-MMC with 2.5% and 5% TiC reinforcement [21]. Hence, copper is a suitable electrode material for EDM of MMCs based on previous research work.

Sidhu et al. utilized Lexicographic Goal Programming (LGP) to optimize the EDM parameters based on the recast layers, surface roughness and material removal rate (MRR) during EDM of Al-6061 composite. Sidhu et al. [22] also analyzed the impact of powder mixed electrical discharge machining (PMEDM) on the microhardness and surface integrity of 65 vol% SiC/A356.2, 30 vol% SiC/A359 and 10 vol% SiC-5 vol% quartz/Al with the Taguchi technique. Singh and Yeh [23] investigated the effect of input parameters during EDM of 6061Al/Al_2O_{3p}/20p aluminum matrix composite (AMC) using the Taguchi technique for multiple responses. Velmurugan [24] selected the central composite rotatable design as a technique to evaluate EDM input variables during machining of Al6061 hybrid MMCs with 4% graphite and 10% SiC particles. Response surface methodology (RSM) was selected to investigate the impact of parameters during EDM of Al7075 with 0.5 wt% B4C nanoparticles [25] and 0.5 wt% SiC nanoparticles [26] as well as an Al-based hybrid MMC (Al6063/SiC/Al_2O_3/Gr) [27]. However, Soft computing techniques are useful when exact mathematical information is not available, and these differ from conventional computing in that it is tolerant of imprecision, uncertainty, partial truth, approximation, and met heuristics.

Adaptive Neuro-Fuzzy Inference System (ANFIS) is one of the soft computing techniques that play a significant role in input-output matrix relationship modeling in EDM of MMCs. ANFIS is a hybrid of fuzzy logic and artificial neural networks (ANNs). It uses the mathematical properties of ANNs to tune rule-based fuzzy systems, which is similar to how humans process information. Hence, ANFIS benefits from the advantages of fuzzy logic and ANNs and overcomes their limitations [28]. It is a hybrid platform which improves the ability to automatically learn from data to solve actual complicated problems. ANFIS is one of the most prominent soft computing methods which can successfully improve prediction outputs. This method is appropriate to reduce redundant input variables and choose the most relevant subset of variables which are truly relevant to outputs. ANFIS can generate the complicated nonlinear relationships between input variables and outputs [29]. ANFIS has been used to model and predict machining outputs based on inputs in different machining processes like wire-EDM [28, 30], micro-EDM [31], milling [32] and turning [33].

Table 1 Chemical composition of Al-20Mg2Si composite produced

Element	Si	Fe	Cu	Mn	Mg	Cr	Ni	Zn	Ti	Al
Wt.%	7.07	0.64	2.034	0.217	12.710	0.034	0.003	0.614	0.001	Bal.

Fig. 1 (a) Induction furnace, (b) melting of Al-20Mg_2Si in 2 kg SiC crucible (top view of induction furnace)

Al-Mg_2Si is a new metal matrix composite and material removal rate in EDM is lower than in other machining processes. Moreover, this is the first attempt to use ANFIS method in order to model MRR in nano-powder mixed EDM (NPMEDM) of MMCs. Hence, one of the aims of this research is to maximize the MRR in NPMEDM of Al-Mg_2Si in situ composite by using ANFIS. Another aim is to validate the ANFIS model with the model generated using RSM. The last aim is to reveal the impact of NPMEDM input variables on the machined surface and microstructure.

2 Experimental details

2.1 Workpiece fabrication

Table 1 represents the chemical composition of Al-20Mg_2Si ingot. The Al-20Mg_2Si composite was produced by melting a commercially available ADC12 alloy (Al-11.7Si-2Cu) using a 2 kg SiC crucible in an induction furnace as shown in Fig. 1. After melting, pure aluminum (99.7 wt%) and pure magnesium (99.9 wt%) were added to adjust the composite composition. After approximately 5 min of waiting for homogenization and dissolution to take place, the melt was skimmed and then carefully poured at 750 ± 5 °C into a mild steel mold that was used to fabricate the workpiece with dimensions of 200 × 100 × 30 mm.

Table 2 Machining parameter levels and symbols

Symbol	Parameters	Unit	Level		
			Low	Center	High
A	Voltage (V)	V	50	80	110
B	Current (I_p)	A	3	9	15
C	Pulse On time (t_{on})	μs	10	105	200
D	Duty factor[a] (D_f)	%	0.25	0.55	0.85

[a] Duty factor $= \frac{\text{Pulse ON time}}{\text{Pulse ON time+Pulse OFF time}} \times 100(\%)$

2.2 Experimental design and procedure

In the present study, an AG40L Sodick EDM machine was utilized to produce 6 mm deep holes on the Al-Mg_2Si in situ composite by using copper electrodes with 5.5 mm diameter and oil-based dielectric fluid mixed with aluminum nano-powder at 1.5 g/lit as it is recommended by Sodick company [34]. Moreover, the positive electrode polarity was selected based on preliminary tests. The current, voltage, duty factor, and pulse ON time were the NPMEDM parameters used to

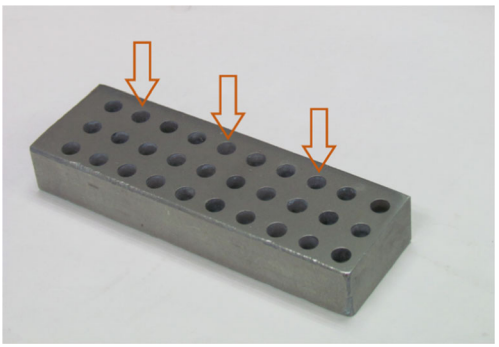

Fig. 2 Machined workpiece under different machining conditions and view angle for microstructural analysis (arrow direction)

Table 3 Experimental design and results

STD	V (V)	I_p (A)	t_{on} (μs)	D_f (%)	Experimental MRR(g/min)	Predicted MRR (g/min)	Residual	Error (%)
1	50	3	10	0.25	0.00642893	0.00643	− 1.07E-06	− 0.017
2	110	3	10	0.25	0.000340654	0.000341	− 3.46E-07	− 0.102
3	50	15	10	0.25	0.0168624	0.0169	− 3.76E-05	− 0.223
4	110	15	10	0.25	0.016706	0.0167	6E-06	0.036
5	50	3	200	0.25	0.000960692	0.000961	− 3.08E-07	− 0.032
6	110	3	200	0.25	0.000115659	0.000116	− 3.41E-07	− 0.295
7	50	15	200	0.25	0.057	0.057	0	0.000
8	110	15	200	0.25	0.0204439	0.0204	4.39E-05	0.215
9	50	3	10	0.85	0.00577697	0.00578	− 3.03E-06	− 0.052
10	110	3	10	0.85	0.000821067	0.000821	6.7E-08	0.008
11	50	15	10	0.85	0.0113396	0.0113	3.96E-05	0.349
12	110	15	10	0.85	0.016479	0.0165	− 2.1E-05	− 0.127
13	50	3	200	0.85	0.000620319	0.00062	3.19E-07	0.051
14	110	3	200	0.85	0.000296006	0.000296	6E-09	0.002
15	50	15	200	0.85	0.0193183	0.0193	1.83E-05	0.095
16	110	15	200	0.85	0.0484091	0.0484	9.1E-06	0.019
17	80	9	105	0.55	0.0273418	0.0273	4.18E-05	0.153
18	50	9	105	0.55	0.0317546	0.0318	− 4.54E-05	− 0.143
19	110	9	105	0.55	0.00273291	0.00273	2.91E-06	0.106
20	80	3	105	0.55	0.00283169	0.00283	1.69E-06	0.060
21	80	15	105	0.55	0.0575487	0.0575	4.87E-05	0.085
22	80	9	10	0.55	0.0141248	0.0141	2.48E-05	0.176
23	80	9	200	0.55	0.0222477	0.0222	4.77E-05	0.214
24	80	9	105	0.25	0.0129597	0.013	− 4.03E-05	− 0.311
25	80	9	105	0.85	0.0262095	0.0262	9.5E-06	0.036
26	83	14.5	105	0.55	0.048563601	0.0486	− 3.6399E-05	− 0.075
27	80	15	200	0.55	0.073608069	0.0736	8.069E-06	0.011

analyze the MRR and microstructure. The experiments were designed by RSM method (27 experiments) comprising 16 two-level factorial design points (=2^4), 1 center point, 8 axial points, and 2 additional points. Then, the ANFIS model was used to analyze the results and generate a 3D graph. The ANFIS model was validated with the model generated using RSM [35]. The MRR was calculated according to the amount of machined workpiece material divided by time of machining. The workpiece weight was measured by a "precision electronic balance" with a 0.0001 g weighing scale. Table 2 displays the machining parameter symbols and levels adopted according to the primary experiments. Spark energy is determined by the amount of electrical power contained in each spark, multiplied by the amount of time the electrical power is flowing. The equation for determining spark energy is [16]:

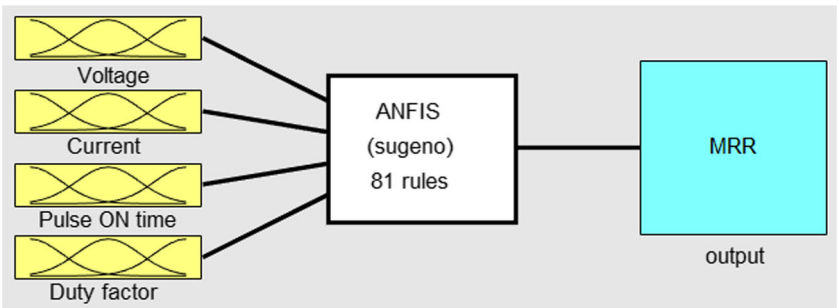

Fig. 3 Adaptive network structure of MRR

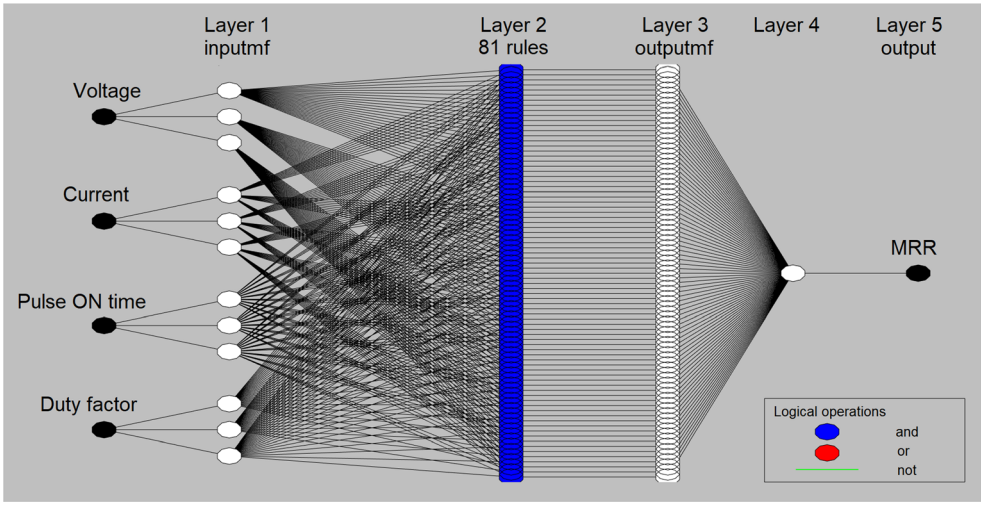

Fig. 4 ANFIS model structure of MRR

$$E = VI_p t_{on} \quad (1)$$

Where E = Spark energy (Watt time (μs)), V = Voltage (V), I_p = Current (A), t_{on} = Pulse ON time (μs).

The non-machined and machined workpieces were prepared for metallography within standard operating procedure for grinding [35]. The ground specimens were then polished with colloidal silica suspension (0.5 μm). Next, 2% HF acid was used to etch the polished samples. Metallographic analysis of the microstructure was carried out using a "Nikon-MIDROPHOT-FXL optical microscope" and a "field emission scanning electron microscopy (FESEM)" equipped with "energy dispersive spectroscopy (EDS)" facilities (Supra-35VP, Carl Zeiss, Germany). XRD (Siemens-D500) was accomplished with a Cu Kα line generated at 35 mA and 40 kV. Figure 2 presents the machined workpiece under different machining conditions and a view angle for microstructural analysis (arrow direction).

3 Results and discussion

3.1 ANFIS model for material removal rate

The material removal rate (MRR) values in Table 3 served as the training dataset to generate the ANFIS model. Figure 3 shows the fuzzy logic designer based on the inputs (current, voltage, pulse ON time, duty factor) and output (MRR). The ANFIS model structure of MRR utilized in this research is shown in Fig. 4. ANFIS employs five network layers to carry out the fuzzy inference steps as represented in Fig. 5: "Layer 1 - input fuzzification", "Layer 2 - fuzzy set database construction", "Layer 3 - fuzzy rule base construction", "Layer 4 - decision-making", and "Layer 5 - output defuzzification" [32, 36, 37].

Layer 1 The degree to which a particular input fulfils the linguistic label considered for the node is the output of the node.

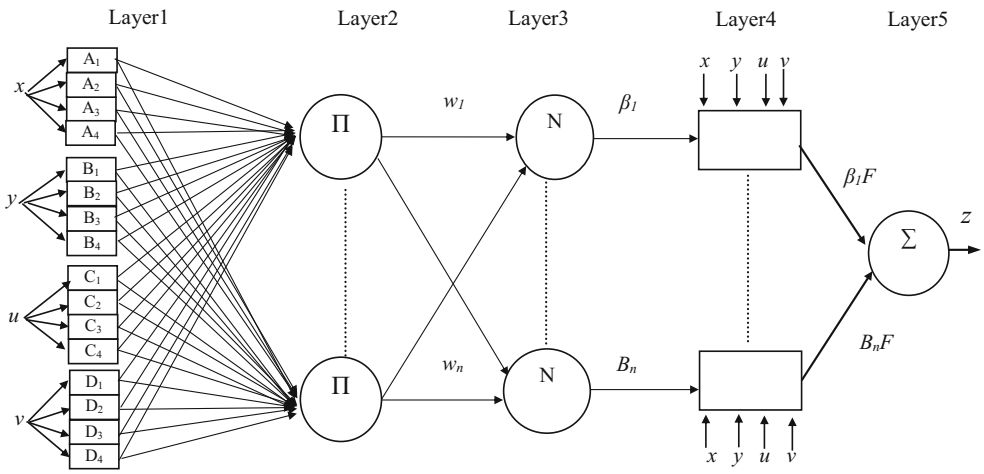

Fig. 5 ANFIS architecture for a Sugeno fuzzy model

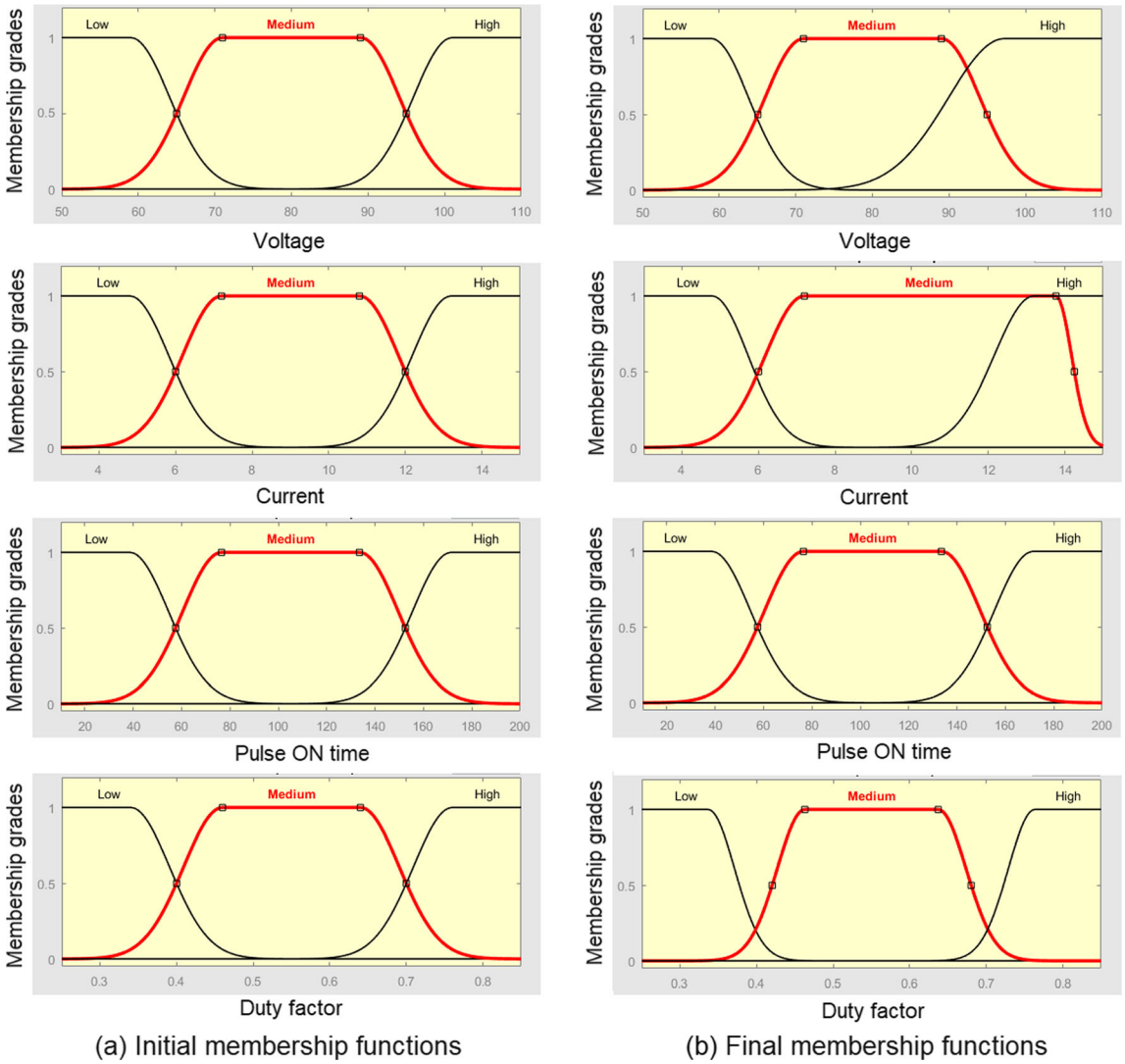

Fig. 6 (a) Initial and (b) final membership function plots of voltage, current, pulse ON time and duty factor

Gauss2mf membership functions are selected to reveal the linguistic terms as the connections between NPMEDM input variables, and MRR is nonlinear.

Membership function of first parameter:

$$A_i(x) = \exp\left[-0.5((x-a_{i1})/b_{i1})^2\right] \quad (2)$$

Membership function of second parameter:

$$B_i(y) = exp\left[-0.5((y-a_{i2})/b_{i2})^2\right] \quad (3)$$

Membership function of third parameter:

$$C_i(u) = exp\left[-0.5((u-a_{i3})/b_{i3})^2\right] \quad (4)$$

Membership function of fourth parameter:

$$D_i(v) = exp\left[-0.5((v-a_{i4})/b_{i4})^2\right] \quad (5)$$

where a_{i1} to a_{i4}, b_{i1} to b_{i4} are the parameter sets.

The gauss2mf functions change because these parameter values are not constant, accordingly representing different membership function forms on linguistic labels A_i, B_i, C_i, and D_i. In this layer, the parameters are labelled as "principle parameters".

Layer 2 Every node calculates the firing strength of its own rule. In this layer, the nodes are labelled "rule nodes" The top and bottom neurons' outputs are as below:

$$Top\ neuron\ w_1 = A_1(x) \times B_1(y) \times C_1(u) \times D_1(v) \quad (6)$$

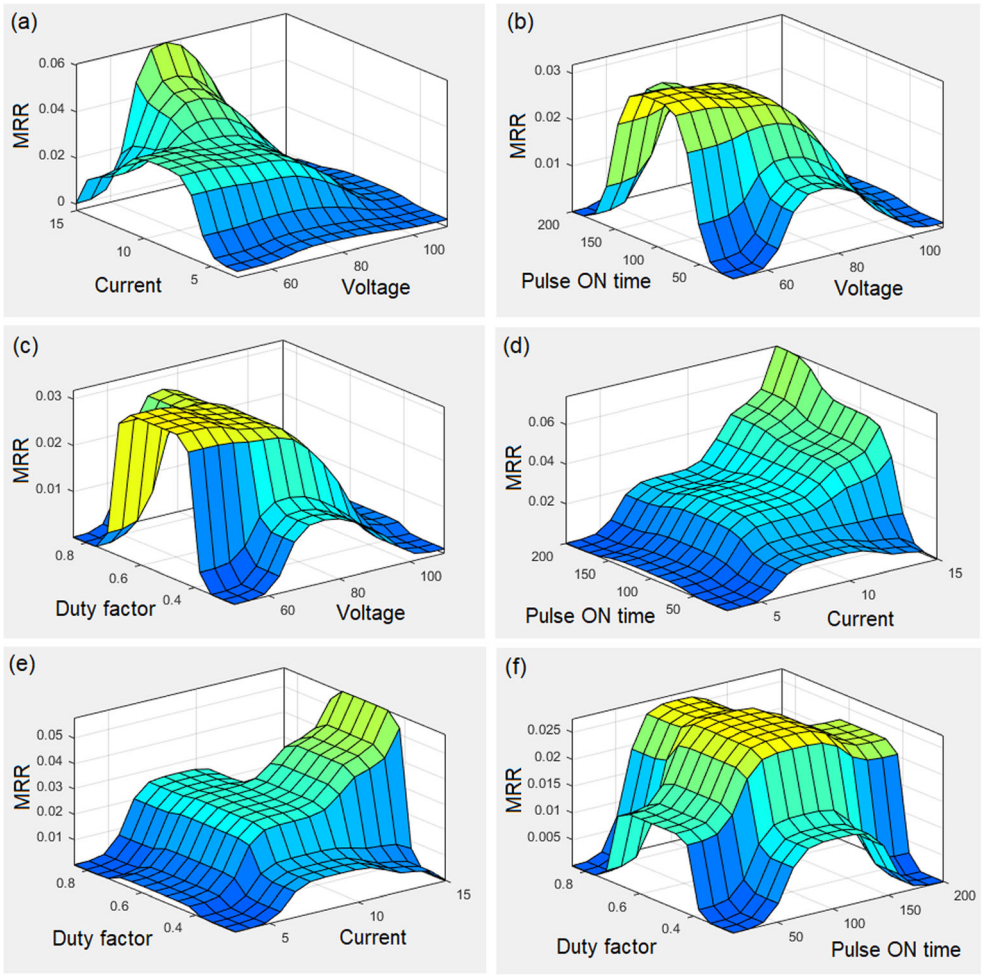

Fig. 7 3D graphs of MRR using ANFIS: (a) voltage-current, (b) voltage-pulse ON time, (c) voltage-duty factor, (d) current-pulse ON time, (e) current-duty factor, (f) pulse ON time-duty factor

$$Second\ neuron\ w_2 = A_1(x) \times B_1(y) \times C_1(u) \times D_2(v) \quad (7)$$

$$Bottom\ neuron\ w_2 = A_4(x) \times B_4(y) \times C_4(u) \times D_4(v) \quad (8)$$

Layer 3 In this layer, N is the label of each node to demonstrate the firing levels' normalization. The top and bottom neurons' output is normalized as bellow:

$$Top\ neuron_1 = w_1/(w_1 + w_2 + ... + w_n) \quad (9)$$

$$Second\ neuron_2 = w_2/(w_1 + w_2 + ... + w_n) \quad (10)$$

$$Bottom\ neuron_n = w_n/(w_1 + w_2 + ... + w_n) \quad (11)$$

Layer 4 The top and bottom neurons' output is the result of the normalized firing level as well as the single-rule output of the first and second rules, respectively.

$$Top\ neuro\, n_1 z_1 = {}_1(a_1 x + b_1 y + c_1 u + d_1 v) \quad (12)$$

$$Second\ neuro\, n_2 z_2 = {}_2(a_2 x + b_2 y + c_2 u + d_2 v) \quad (13)$$

$$Bottom\ neuro\, n_n z_n = {}_n(a_n x + b_n y + c_n u + d_n v) \quad (14)$$

Layer 5 In this layer, the individual node calculates the general system output as the total of all incoming signals, i.e.

$$z = {}_1 z_1 + {}_2 z_2 \ldots + {}_n z_n \quad (15)$$

The hybrid neural net parameters (that specify the membership function shape of the premises) are trained by descent-type means if a crisp training set $\{(x^k, y^k, u^k, v^k)\ k = 1,\ldots,k\}$ c is used. The error function for pattern k is calculated by:

$$E_k = \left(o^k - z^k\right)^2 \quad (16)$$

Where z^k is the output calculated by the hybrid neural net and o^k is the real output [5].

Three levels including low, medium, and high can be considered in order to show the membership functions of each input variable through the architecture. Figure 6 illustrates the initial and final membership function plots of the four

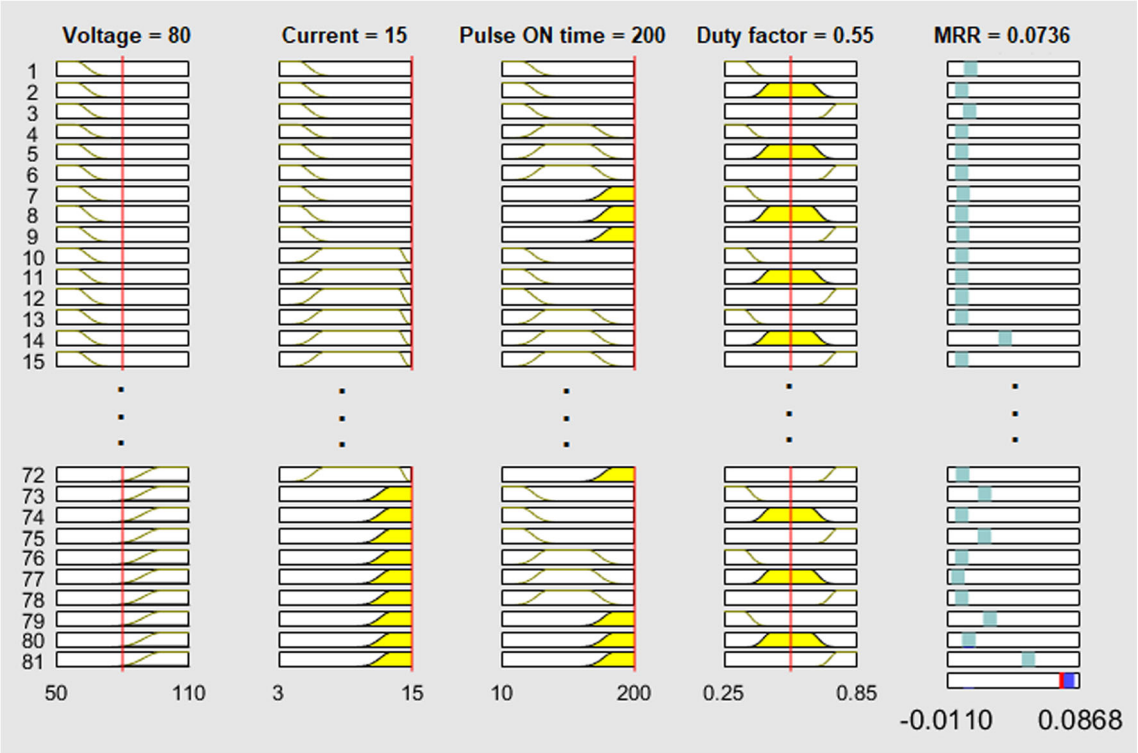

Fig. 8 Fuzzy rule viewer of ANFIS prediction of MRR based on NPMEDM parameters

NPMEDM input variables resulting from training via gauss2mf. The changes in the final membership function shape after training reveal that current has the most significant effect, followed by voltage, pulse ON time and duty factor.

Figure 7 demonstrates the 3D graphs for MRR based on all NPMEDM parameters. The interactions of current-voltage and current-pulse ON time have the highest effect on the MRR among all of the interactions, followed by the current-pulse ON time interaction, as represented in Fig. 7. The discharge gap between workpiece and electrode is adjusted by the voltage [38] and increases by increasing the voltage. Based on Fig. 7(a) band (c), high MRR is achievable when the voltage is around 80 V (middle range) because the gap voltage is in a suitable range based on other NPMEDM parameters, and the debris and chips can be removed easily from the gap between the workpiece and electrode. It is obvious from Fig. 7 that current has the most significant impact on MRR. Figure 7 (a, d, and e) shows that MRR augments remarkably with amplification of current due to the augmentation of spark energy [15]. MRR is reduced with increasing voltage beyond 80 V, as the gap between workpiece and electrode is larger than a suitable value. The effect of the current-pulse ON time interaction (Fig. 7(d)) is much higher that the effect of the voltage-pulse ON time and pulse ON time-duty factor interactions (Fig. 7(b) and (f)). Hence, selecting the current-pulse ON time interaction (Fig. 7(d)) is the best way to interpret the impact of pulse ON time on MRR. It is clear from Fig. 7(d) that when the current is approximately 3 A (low level), the MRR increase trend is very slow with rising pulse ON time. However, when the current is approximately 15 A (high level), the rising pulse ON time has the highest impact on MRR. Thus, augmenting the pulse ON time leads to enhanced MRR because the spark energy rises [27] as well. On the other hand, the duty factor has the least impact on MRR among all NPMEDM parameters. Figure 7(c, e, and f) illustrates that high MRR is achievable when the duty factor is approximately in the middle range. This is because pulse OFF time is in a suitable range and there is enough time to solidify the chips and debris and remove them from the gap between the workpiece and electrode as well as deionize the dielectric.

Based on the above, it can be concluded that current has the most significant effect, followed by voltage, pulse ON time and duty factor. Moreover, the interactions of current-voltage and current-pulse ON time have the highest effect on MRR among all interactions, followed by the current-pulse ON time interaction. In addition, this result is quite similar to a previous publication by the authors [35], where voltage, current, the two-level interaction of current and voltage, the second-order effect of voltage and two-level interaction of current and pulse ON time are the most significant factors on MRR. Finally, the highest MRR can be achieved when pulse ON time and current are at high levels (200 μs and 15 A) as well as

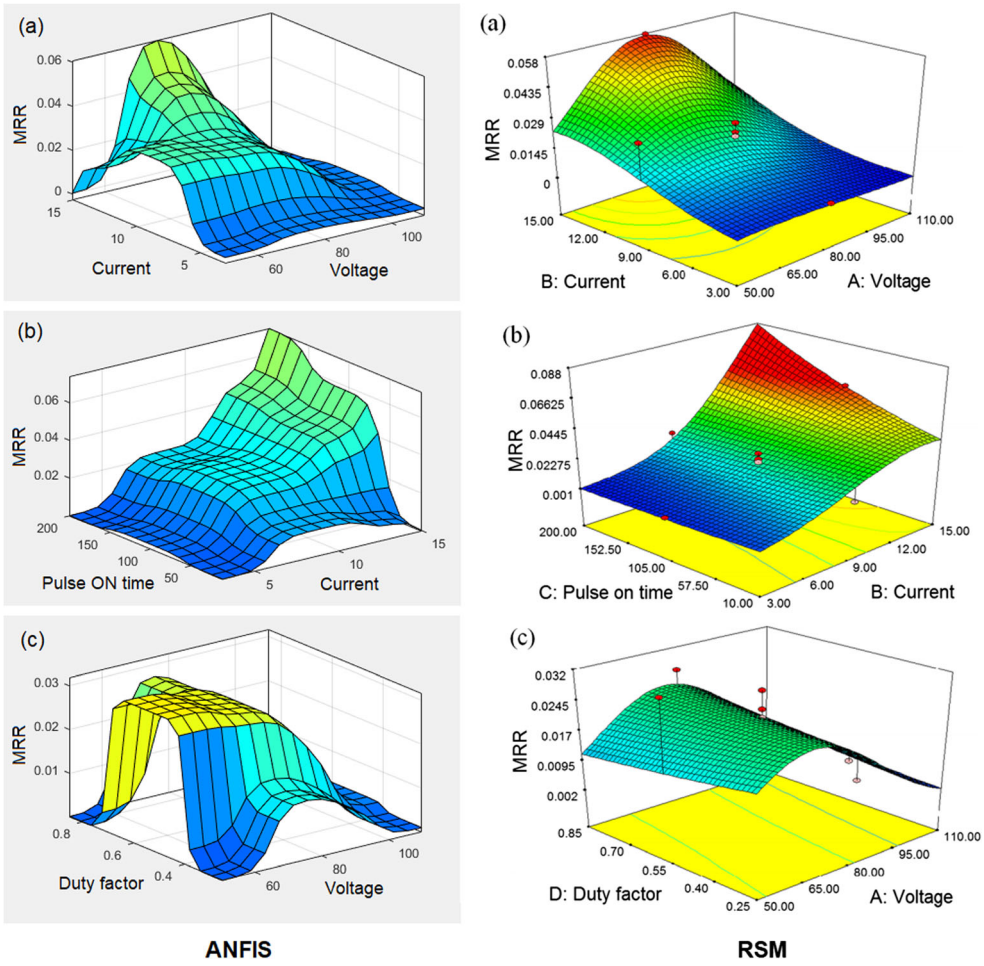

Fig. 9 3D graphs of MRR based on current-voltage, current-pulse ON time and voltage-duty factor using ANFIS (a-c) and RSM (a-c) methods [35]

when the voltage and duty factor are in middle ranges (around 80 V and 0.55%).

Figure 8 represents the fuzzy rule viewer of ANFIS model of MRR prediction based on NPMEDM parameters. The MRR predicted was 0.0736 g/min from the fuzzy rule viewer in Fig. 8 when the voltage was 80 V, the current 15 A, the pulse ON time 200 μs and the duty factor 0.55%. Table 3 compares the actual MRR and predicted MRR. It is clear that there are small dereferences between actual MRR and predicted MRR. The highest value of error is 0.349% which is very low and desirable because more accurate prediction of MRR can be achieved with lower error. Hence, the predicted values of MRR in NPMEDM of Al-Mg2Si MMC are very accurate.

Figure 9 shows 3D graphs of MRR based on current-voltage, current-pulse ON time and voltage-duty factor using ANFIS (a-c) and RSM (a-c). In Fig. 9, the 3D graphs of MRR generated by ANFIS (ANFIS a, b, and c) are validated with the graphs generated by RSM (RSM a, b, and c) in a previous publication [35]. It is clear that the 3D graphs generated by both methods are almost similar. The small difference between the 3D graphs is logical, because the analysis process with ANFIS is totally different from RSM. Hence, the ANFIS

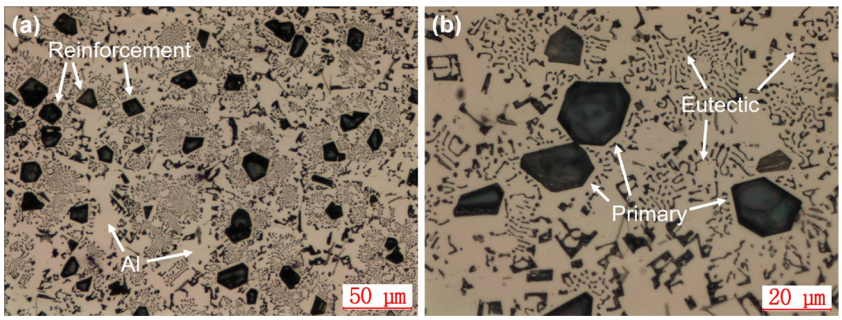

Fig. 10 Optical micrographs of Al-20Mg_2Si composite before NPMEDM at (a) low and (b) high magnification

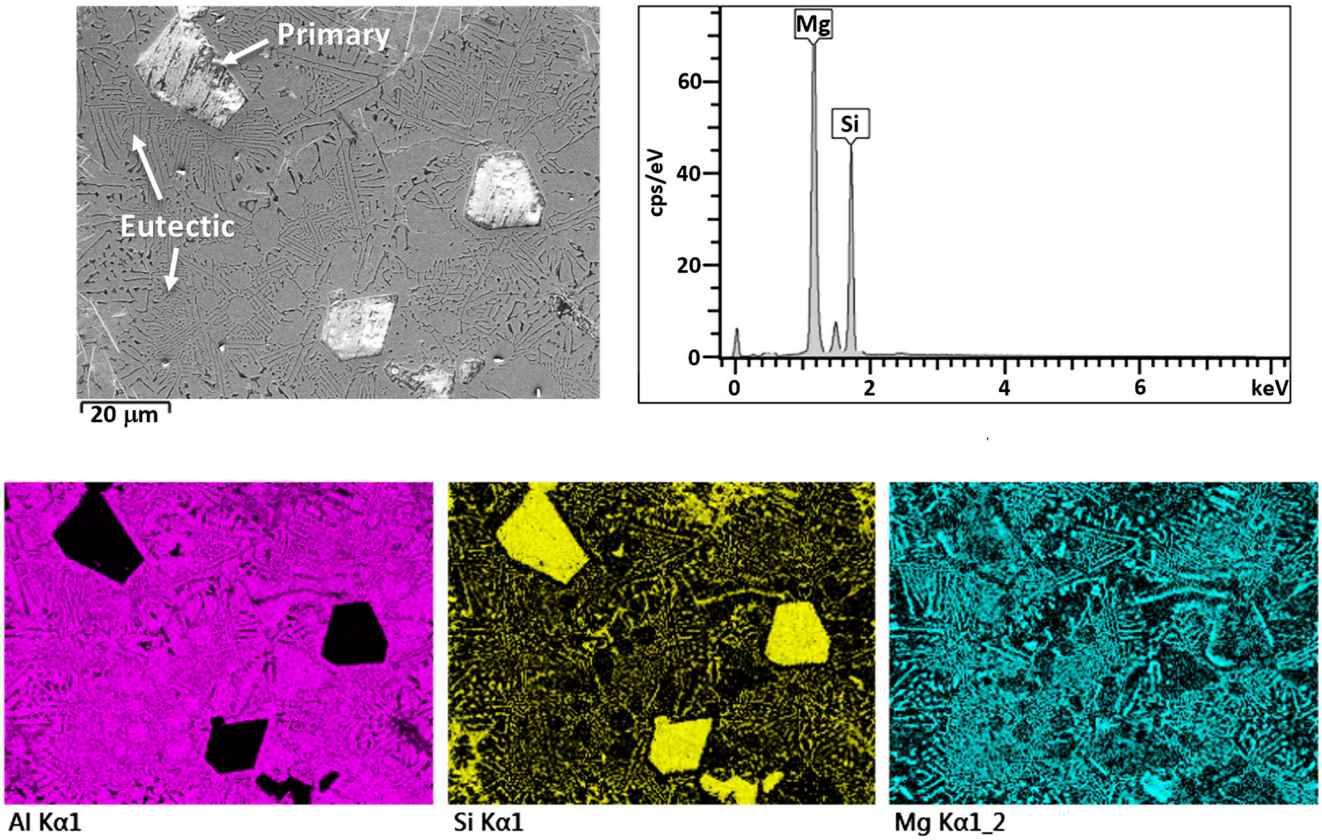

Fig. 11 SEM micrograph with corresponding elemental mapping of Al-20Mg_2Si composite and EDS profile of Mg_2Si particles

model is validated for MRR prediction in NPMEDM of Al-20Mg_2Si composite.

3.2 Microstructure characterization before NPMEDM

Figure 10 illustrates the microstructure of Al-20Mg_2Si composite before NPMEDM at low and high magnification. In addition, Fig. 11 shows SEM micrograph with the corresponding elemental mapping of as-cast Al-20Mg_2Si composite. The EDS profile of particles observed in Fig. 11 reveals that in the molecular structure of Mg_2Si particles the atomic ratio of Mg is approximately twice that of Si. As seen in Figs. 10 and 11, the microstructure comprises primarily Mg_2Si particles and eutectic Mg_2Si with a mostly lamellar morphology as marked in Fig. 11. The elemental mapping shows the distribution of Al, Mg, and Si elements in the microstructure. The properties of the composite are mostly correlated to the reinforcement particles embedded in the aluminum matrix. The size, shape, and distribution of primary Mg_2Si particles are important factors affecting the mechanical properties and machinability of the fabricated composite. Moreover, Fig. 12 illustrates the composite's XRD pattern, which indicates the existence of Mg_2Si and aluminum phases in the fabricated Al-20Mg_2Si composite.

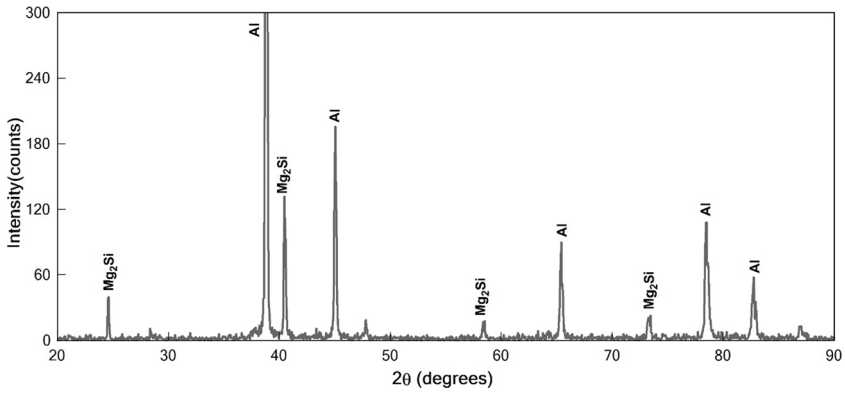

Fig. 12 XRD pattern of as-cast Al-20Mg_2Si composite

3.3 Microstructure characterization after NPMEDM

The spark energy rises with the augmentation of pulse ON time, current and voltage, whereas the duty factor has no effect on the spark energy based on the equation for computing spark energy ($E = VI_p t_{on}$ [16]) [15]. In addition, the discharge gap between the workpiece and electrode augments with rising voltage, because the discharge gap is adjusted by the voltage [35]. Selecting an appropriate voltage based on the duty factor, pulse ON time and current leads to higher MRR and can help the spark energy reach the workpiece. MRR enhances with increasing voltage up to an optimum value when the pulse ON time and current are at high levels because the discharge gap increases and debris can be removed easily from the discharge gap. Meanwhile, MRR is reduced with increasing voltage beyond the desired range as the discharge gap exceeds the appropriate value and the workpiece receives less spark energy [35].

Figure 13 illustrates cross sections of the surfaces machined at various NPMEDM parameters. Figure 13 shows the microstructure and surface of a machined workpiece in various machining conditions. In Fig. 13, by comparing the low voltage (experiments 1, 3, 5, 7, 9, 11, 13, and 15) and high voltage (experiments 2, 4, 6, 8, 10, 12, 14, and 16) at the same pulse ON time, current and duty factor, higher voltage apparently produces bigger craters and a non-uniform surface in the

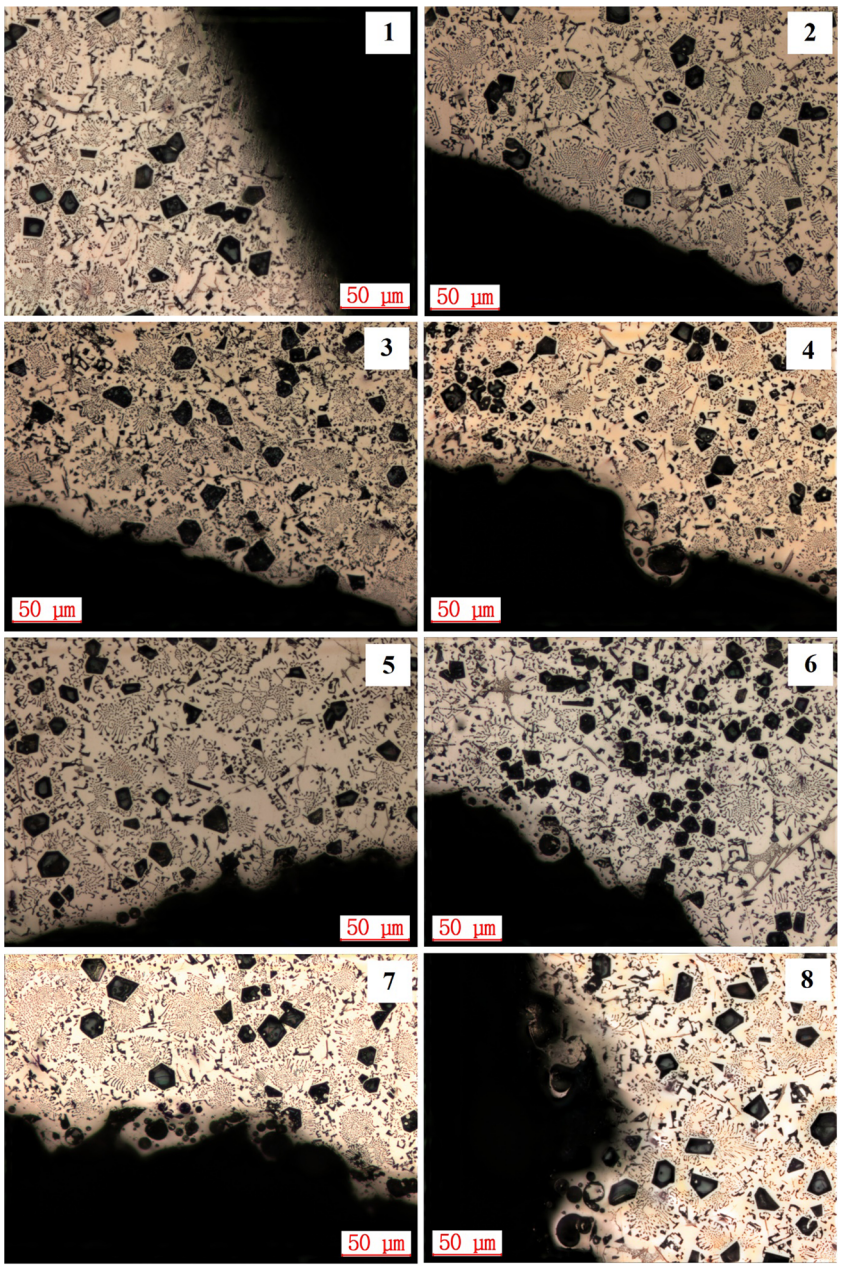

Fig. 13 Microstructure of machined Al-20Mg_2Si (experiments 1–16)

machined region owing to the augmented spark energy [15] and discharge gap [35]. Hence, the machined surface deteriorates with increasing voltage. Evidently, the size of craters increases when the current rises from 3 A (experiments 1, 2, 5, 6, 9, 10, 13 and 14) to 15 A (experiments 3, 4, 7, 8, 11, 12, 15 and 16) as the spark energy increases. Changing the pulse ON time from 10 μs (experiments 1–4 and 9–12) to 200 μs (experiments 5–8 and 13–16) leads to a rise in spark energy, bigger craters and the rougher surface. The duty factor does not have a remarkable impact on the surface produced when it rises from 0.25% (experiments 1–8) to 0.85% (experiments 9–16). The worst profile uniformity is obtained in experiments 15 and 16 when the voltage, pulse ON time and current are high. Figure 14 shows the effects of EDM parameters on the spark energy, size of craters, and MRR based on the results achieved. Hence, changing the NPMEDM parameters only influences the microstructure in the machined region (recast layer) and has no effect on other areas. Moreover, the recast layer thickness depends on spark energy, whereby a decrease in spark energy leads to less microstructural change and recast layer thickness.

NPMEDM parameters exhibit three different effects on Mg_2Si reinforcement, including spalling, cut-off and the aluminum layer covering the Mg_2Si reinforcement, as shown in Fig. 15. In Fig. 15(a), Mg_2Si reinforcement spalling from the aluminum (Al) matrix is observed. Figure 15(b) shows how an

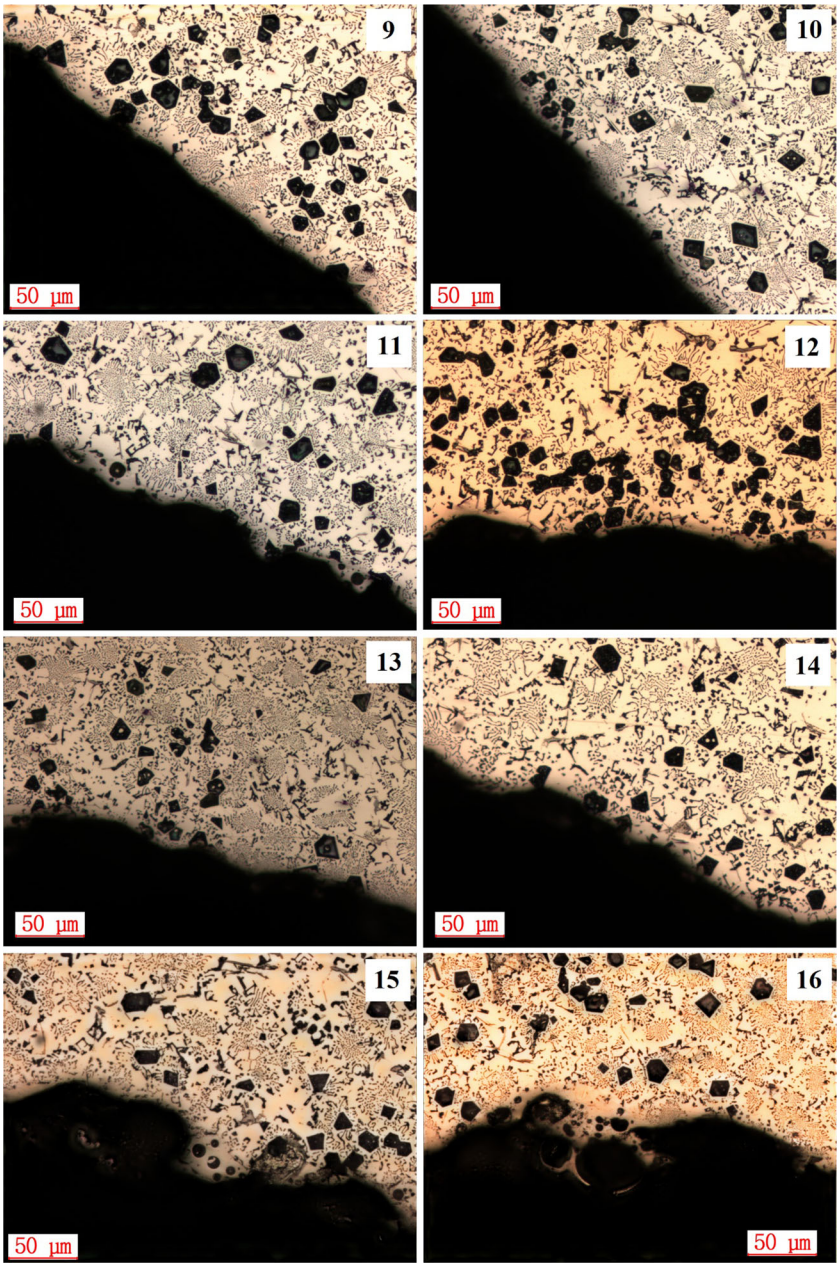

Fig. 13 continued.

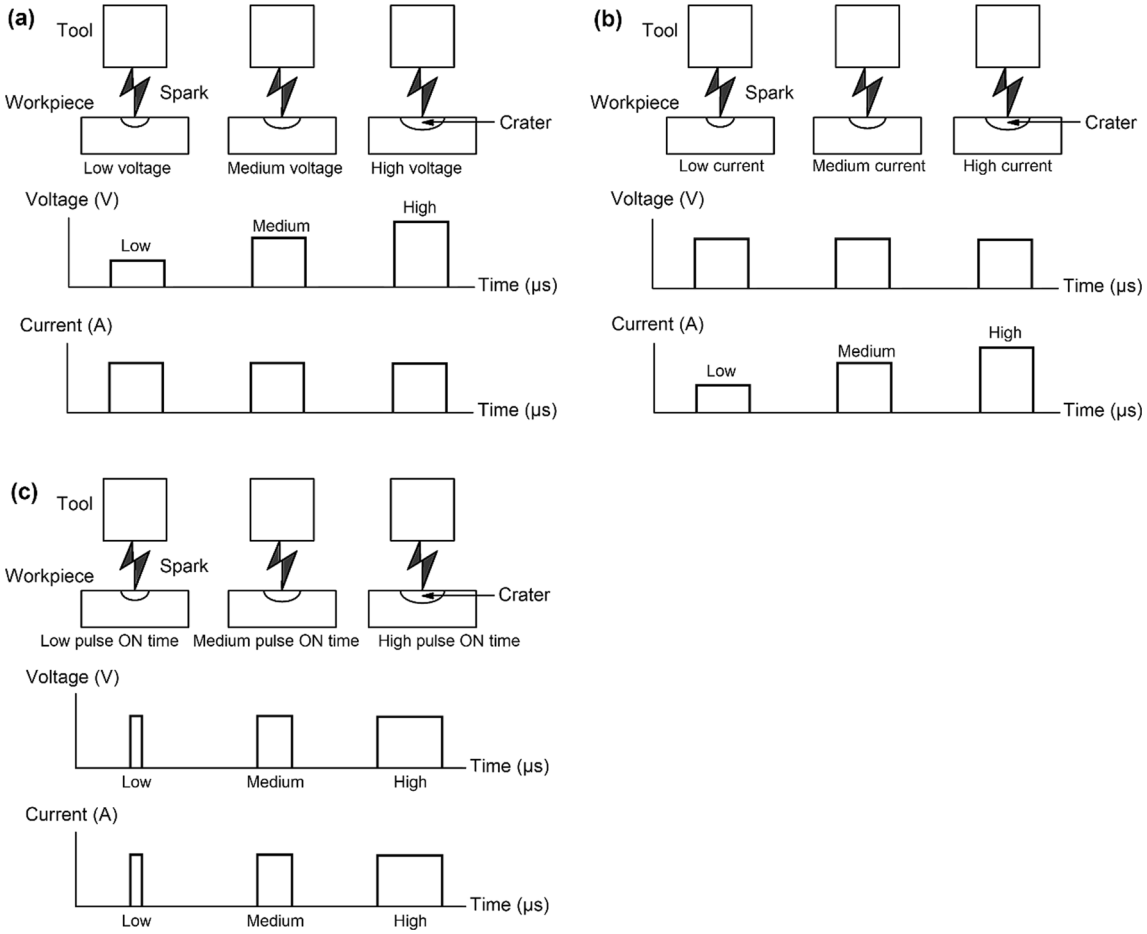

Fig. 14 Effects of EDM parameters on the spark energy, size of craters, and MRR

Al layer covers the Mg_2Si reinforcement and reinforcement cut-off is observed on the machined surface.

4 Conclusion

In this work, the effects of NPMEDM input variables were analyzed on MRR and microstructural changes during NPMEDM of Al-Mg_2Si in situ composite. The ANFIS model of MRR was validated by the generated model with the RSM method. According to the ANFIS model of MRR, the interactions of current-voltage and current-pulse ON time had the most significant effect on MRR among all interactions. Current was the most effective, followed by voltage, pulse ON time and duty factor. The highest MRR was achieved when pulse ON time and current were high (200 μs and 15 A) and the voltage and duty factor were in middle ranges (around 80 V and 0.55%). An analysis of the Al-Mg_2Si microstructure demonstrated that pulse ON time, current and voltage had remarkable effects on the

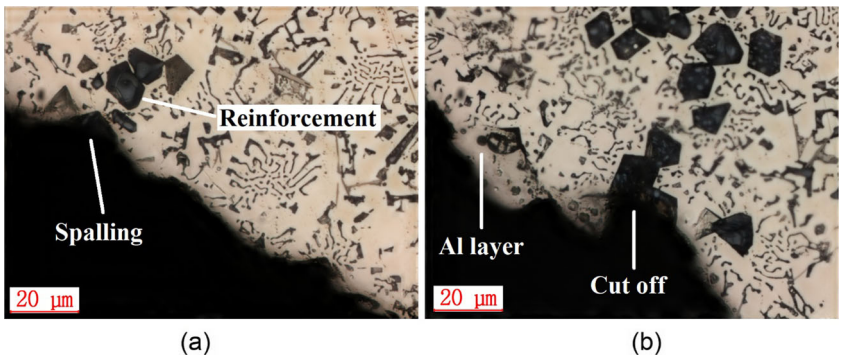

Fig. 15 Effects of NPMEDM parameters on Mg_2Si reinforcement: (a) Spalling at 110 V, 3 A, 10 μs, 0.25%, (b) Al layer and cut-off at 110 V, 3 A, 200 μs, 0.25%

microstructure, size of craters, and profile of the machined surface and has no effect on other areas. Moreover, decrease in spark energy leads to less microstructural change and better surface finish.

Acknowledgments The authors would like to acknowledge both of University of Malaya and King Fahd University of Petroleum & Minerals for providing support.

References

1. Jahangiri A, Idris MH, Farahany S (2013) Investigation on tungsten inert gas welding of in situ Al-15 and 20 Mg2Si composites with an Al-Si filler. J Compos Mater 47(10): 1283–1291
2. Qin Q, Zhao Y, Xiu K, Zhou W, Liang Y (2005) Microstructure evolution of in situ Mg_2Si /Al–Si–Cu composite in semisolid remelting processing. Mater Sci Eng A 407(1):196–200
3. Razavykia A, Farahany S, Yusof NM (2015) Evaluation of cutting force and surface roughness in the dry turning of Al–Mg2Si in-situ metal matrix composite inoculated with bismuth using DOE approach. Measurement 76:170–182
4. Kılıçkap E, Çakır O, Aksoy M, İnan A (2005) Study of tool wear and surface roughness in machining of homogenised SiC-p reinforced aluminium metal matrix composite. J Mater Process Technol 164-165:862–867
5. Hourmand M, Sarhan AA, Sayuti M (2017) Micro-electrode fabrication processes for micro-EDM drilling and milling: a state-of-the-art review. Int J Adv Manuf Technol 91(1–4): 1023–1056
6. Flaño O, Ayesta I, Izquierdo B, Sánchez JA, Zhao Y, Kunieda M (2018) Improvement of EDM performance in high-aspect ratio slot machining using multi-holed electrodes. Precis Eng 51:223–231
7. Nakagawa T, Yuzawa T, Sampei M, Hirata A (2017) Improvement in machining speed with working gap control in EDM milling. Precis Eng 47:303–310
8. Hourmand M, Sarhan AAD, Noordin MY (2017) Development of new fabrication and measurement techniques of micro-electrodes with high aspect ratio for micro EDM using typical EDM machine. Measurement 97:64–78
9. Hourmand M, Noordin MY (2014) Micro-electrode fabrication process using EDM. Adv Mater Res 845:980–984
10. Daud ND, AbuZaiter A, Leow PL, Ali MSM (2018) The effects of the silicon wafer resistivity on the performance of microelectrical discharge machining. Int J Adv Manuf Technol 95(1–4):257–266
11. Mohal S, Kumar H (2017) Parametric optimization of multiwalled carbon nanotube-assisted electric discharge machining of Al-10% SiCp metal matrix composite by response surface methodology. Mater Manuf Process 32(3):263–273
12. Singh B, Kumar J, Kumar S (2016) Investigation of the tool wear rate in tungsten powder-mixed electric discharge machining of AA6061/10% SiCp composite. Mater Manuf Process 31(4):456–466
13. Assarzadeh S, Ghoreishi M (2013) A dual response surface-desirability approach to process modeling and optimization of Al2O3 powder-mixed electrical discharge machining (PMEDM) parameters. Int J Adv Manuf Technol 64(9–12):1459–1477
14. Kung K-Y, Horng J-T, Chiang K-T (2009) Material removal rate and electrode wear ratio study on the powder mixed electrical discharge machining of cobalt-bonded tungsten carbide. Int J Adv Manuf Technol 40(1–2):95–104
15. Hourmand M, Sarhan AAD, Noordin MY, Sayuti M (2017) 1.10 Micro-EDM drilling of tungsten carbide using microelectrode with high aspect ratio to improve MRR, EWR, and hole quality A2 - Hashmi, MSJ. In: Comprehensive materials finishing. Elsevier, Oxford, pp 267–321
16. Jameson EC (2001) Electrical discharge machining. In: Society of Manufacturing Engineers. Dearbern, Michigan
17. Pramanik A (2014) Developments in the non-traditional machining of particle reinforced metal matrix composites. Int J Mach Tools Manuf 86:44–61
18. Kumar SV, Kumar MP (2015) Machining process parameter and surface integrity in conventional EDM and cryogenic EDM of Al–SiCp MMC. J Manuf Process 20:70–78
19. Seo Y, Kim D, Ramulu M (2006) Electrical discharge machining of functionally graded 15–35 vol% SiCp/Al composites. Mater Manuf Process 21(5):479–487
20. Daneshmand S, Masoudi B (2017) Investigation of weight percentage of alumina fiber on EDM of Al/Al2O3 metal matrix composites. Silicon 10(3):1003–1011
21. Senthilkumar V, Omprakash BU (2011) Effect of titanium carbide particle addition in the aluminium composite on EDM process parameters. J Manuf Process 13(1):60–66
22. Sidhu SS, Batish A, Kumar S (2013) Study of surface properties in particulate reinforced MMC using powder-mixed EDM. Mater Manuf Process 29(1):46–52
23. Singh S, Yeh M-F (2012) Optimization of abrasive powder mixed EDM of aluminum matrix composites with multiple responses using gray relational analysis. J Mater Eng Perform 21(4):481–491
24. Velmurugan C, Subramanian R, Thirugnanam S, Ananadavel B (2011) Experimental investigations on machining characteristics of Al 6061 hybrid metal matrix composites processed by electrical discharge machining. Int J Eng Sci Technol 3(8):87–101
25. Gopalakannan S, Senthilvelan T (2013) A parametric study of electrical discharge machining process parameters on machining of cast Al/B4C metal matrix nanocomposites. Proc Inst Mech Eng B J Eng Manuf
26. Gopalakannan S, Senthilvelan T (2013) EDM of cast Al/SiC metal matrix nanocomposites by applying response surface method. Int J Adv Manuf Technol 67(1–4):485–493
27. Kumar R, Singh I, Kumar D (2013) Electro discharge drilling of hybrid MMC. Procedia Eng 64:1337–1343
28. Çaydaş U, Hasçalık A, Ekici S (2009) An adaptive neuro-fuzzy inference system (ANFIS) model for wire-EDM. Expert Syst Appl 36(3, Part 2):6135–6139
29. Yadegaridehkordi E, Hourmand M, Nilashi M, Shuib L, Ahani A, Ibrahim O (2018) Influence of big data adoption on manufacturing companies' performance: an integrated DEMATEL-ANFIS approach. Technol Forecast Soc Chang 137:199–210. https://doi.org/10.1016/j.techfore.2018.07.043
30. Maher I, Sarhan AAD, Marashi H, Barzani MM, Hamdi M (2016) White layer thickness prediction in wire-EDM using CuZn-coated wire electrode—ANFIS modelling. Trans IMF 94(4):204–210
31. Suganthi XH, Natarajan U, Sathiyamurthy S, Chidambaram K (2013) Prediction of quality responses in micro-EDM process using an adaptive neuro-fuzzy inference system (ANFIS) model. Int J Adv Manuf Technol 68(1–4):339–347
32. Maher I, Eltaib MEH, Sarhan AAD, El-Zahry RM (2015) Cutting force-based adaptive neuro-fuzzy approach for accurate surface roughness prediction in end milling operation for intelligent machining. Int J Adv Manuf Technol 76(5–8):1459–1467
33. Aydın M, Karakuzu C, Uçar M, Cengiz A, Çavuşlu MA (2013) Prediction of surface roughness and cutting zone temperature in

dry turning processes of AISI304 stainless steel using ANFIS with PSO learning. Int J Adv Manuf Technol 67(1–4):957–967
34. Instruction Manual. Sodick Wire-Cut EDM PGM WHITE 3 AG Series (Version 2.0)
35. Hourmand M, Farahany S, Sarhan AA, Noordin MY (2015) Investigating the electrical discharge machining (EDM) parameter effects on Al-Mg2Si metal matrix composite (MMC) for high material removal rate (MRR) and less EWR–RSM approach. Int J Adv Manuf Technol 77(5–8):831–838
36. Lo S-P (2003) An adaptive-network based fuzzy inference system for prediction of workpiece surface roughness in end milling. J Mater Process Technol 142(3):665–675
37. Jang J-SR, Sun C-T, Mizutani E (1997) Neuro-fuzzy and soft computing; a computational approach to learning and machine intelligence
38. Egashira K, Matsugasako A, Tsuchiya H, Miyazaki M (2006) Electrical discharge machining with ultralow discharge energy. Precis Eng 30(4):414–420